Smoke plume height measurement of prescribed burns in the south-eastern United States

Yongqiang Liu[A,B], *Scott L. Goodrick*[A], *Gary L. Achtemeier*[A], *Ken Forbus*[A] *and David Combs*[A]

[A]USDA Forest Service, Center for Forest Disturbance Science, 320 Green Street, Athens, GA 30602, USA.
[B]Corresponding author. Email: yliu@fs.fed.us

Abstract. Smoke plume height is important for modelling smoke transport and resulting effects on air quality. This study presents analyses of ceilometer measurements of smoke plume heights for twenty prescribed burns in the south-eastern United States. Measurements were conducted from mid-winter to early summer between 2009 and 2011. Approximately half of the burns were on tracts of land over 400 ha (1000 acres) in area. Average smoke plume height was ~1 km. Plume height trended upward from winter to summer. These results could be used as an empirical guideline for fire managers to estimate smoke plume height in the south-eastern US when modelling and measurement are not available. The average could be used as a first-order approximation, and a second-order approximation could be obtained by using the average for spring and autumn seasons, and decreasing or increasing by 0.2 km the average for winter or summer. The concentrations of particulate matter with an aerodynamic diameter less than 2.5 or 10 μm ($PM_{2.5}$ and PM_{10}) within smoke plumes calculated from ceilometer backscatter are ~80 and 90 μg m^{-3}, and trend downward from winter to summer. Large smoke concentrations are found in the lower portion of smoke plumes for many burns. Smoke plume height shows fast and uniform fluctuations at minute scales for almost all burns and slow and irregular fluctuations at scales from tens of minutes to hours for some burns.

Additional keywords: ceilometer measurement, particulate matter concentration.

Received 19 May 2011, accepted 16 July 2012, published online 24 September 2012

Introduction

Smoke plume height (also known as smoke plume rise, or smoke plume final rise in some early studies) is the height where vertical ascent of a smoke plume ceases. Smoke plume heights range from hundreds of metres for prescribed fires to thousands of metres for wildfires. Plume height is an important factor for local and regional smoke transport and air-quality modelling. Fire emissions, if injected to higher elevations, can be transported out of rural burn sites to affect air quality at distant highly populated urban areas. Smoke plume height is a required input for many regional air-quality models. The Community Multiscale Air Quality (CMAQ) model (Byun and Ching 1999; Byun and Schere 2006), for example, uses the Sparse Matrix Operator Kernel Emissions (SMOKE) modelling system (Houyoux *et al.* 2002) to provide plume height as part of initial and boundary conditions for elevated emission sources. The BlueSky wildfire smoke modelling system (Larkin *et al.* 2009) also includes algorithms for smoke plume height calculation in order to determine the downwind smoke concentrations and effects on air quality.

In the early smoke modelling applications of CMAQ and SMOKE, the Briggs scheme (Briggs 1975) was used to calculate smoke plume height. The Briggs scheme (Briggs 1975) is a two-thirds power law integral model based on differential equations governing mass, momentum and energy fluxes through a plume cross-section (Weil 1988). The calculated plume height is determined by both emission properties, such as initial buoyancy flux and exit velocity, and ambient properties, such as wind and thermal stability. The two-thirds power law is formulated on the assumption that plume buoyancy flux dominates plume momentum flux (not the ambient mechanical turbulence), thus in theory if the plume momentum flux dominates, the formula will not perform well. Guldberg (1975) compared the accuracy of the Briggs scheme (Briggs 1975) with two other schemes in modelling the heights of hot, buoyant plumes and found that the Briggs scheme (Briggs 1975) best predicted the observed plume heights during periods of low wind speed.

In comparison with a single power plant stack, on which the Briggs plume rise scheme (Briggs 1975) is based, forest burning has multiple-core plumes, which are usually more buoyant and involve stronger atmospheric entrainment. In addition, mechanical turbulence generated at the ground surface can be of similar magnitude to the buoyantly produced turbulence for weak forest fires, especially a prescribed burn under windy conditions. These differences lead to potential problems with the application of the Briggs scheme (Briggs 1975) to fire smoke plume height modelling. For example, the National Oceanic and Atmospheric Administration's Smoke Forecasting System

showed a tendency to over-predict the measured $PM_{2.5}$ (particulate matter with an aerodynamic diameter less than 2.5 μm) concentrations in the western United States between September 2006 and November 2007 (Stein *et al.* 2009), and this prediction was shown to be very sensitive to the injection height of fire emissions calculated using the Briggs scheme (Briggs 1975).

The problems with the Briggs scheme (Briggs 1975) for fire application emphasise the importance in developing smoke plume height schemes specifically for wildfires and prescribed fires. Efforts have been made recently that led to the development of several smoke plume models with various levels of complexity. Harrison and Hardy (2002) developed an empirical model to estimate plume rise using maximum flame power (power of a flame is a measure of the total radiative energy leaving the surface of the fire in unit time) based on the measurement of a large number of prescribed burns in the north-western United States (Hardy *et al.* 1993). Pouliot *et al.* (2005) modified the Briggs scheme (Briggs 1975) by converting the heat flux from each fire to a buoyancy flux suitable for use with the Briggs plume rise algorithm (Briggs 1975). The Western Regional Air Partnership (Western Regional Air Partnership 2005) used a climatological method by specifying pre-defined plume bottom and plume top and a pre-defined diurnal temporal profile for each fire. The modified Briggs scheme (Briggs 1975) and the WRAP climatological method have been incorporated into SMOKE. Freitas *et al.* (2007) developed a model to explicitly simulate smoke plume height based on a one-dimensional dynamic entrainment plume model (Latham 1994). It was modified later to include the effects of winds (Freitas *et al.* 2010). An extended set of equations, including the horizontal motion of the plume and the additional increase of the plume size, was solved to explicitly simulate the time evolution of plume height and determine the final injection layer. This model has been incorporated into the WRF-Fire modelling system and evaluated for individual wildfire events (Grell *et al.* 2011; Mandel *et al.* 2011). WRF-Fire combines the Weather Research and Forecasting (WRF) model (Skamarock *et al.* 2008) with a surface fire behaviour model for calculating fire spread rate using fuel properties, wind velocities from WRF, and terrain slope. WRF-Fire allows modelling of the growth of a wildland fire and the dynamic feedbacks with the atmosphere.

Prescribed burning is an important tool for forest and wildlife management, including managing rare and endangered plants and animals, while reducing the buildup of fuels and the risk of destructive wildfire. Approximately $2 \times 10^6 – 3 \times 10^6$ ha ($6 \times 10^6 – 8 \times 10^6$ acres) of forest and agricultural lands are burned each year in the southern United States (Wade *et al.* 2000). In comparison with wildfires, buoyancy generated by prescribed fires is smaller because there is typically less heat released. Achtemeier *et al.* (2011) developed a dynamical-stochastic smoke plume model (Daysmoke) specifically for prescribed fires. Based on ASHFALL (Achtemeier 1998), a plume model for deposition of ash from sugarcane fires, Daysmoke includes an entraining turret plume sub-model, a detraining particle trajectory sub-model, a convective circulation parameterisation and an emissions production sub-model. Daysmoke has been incorporated into SHRMC-4S, a framework for simulating smoke and air quality effects of prescribed burning (Liu *et al.* 2009).

Smoke plume measurement is essential for validating smoke models. Several smoke detection techniques are available for measuring smoke plume height. Weather radars such as the Weather Surveillance Radar-1988 Doppler (WSR-88D) in the US national network have historically been used to detect smoke plume reflectivity and structure (e.g. Banta *et al.* 1992; Rogers and Brown 1997; Jones and Christopher 2008; Melnikov *et al.* 2008; Tsai *et al.* 2009). LiDAR (light detection and ranging) is well adapted for smoke detection (e.g. Pershin *et al.* 1999; Mikkelsen *et al.* 2002; Lavrov *et al.* 2003; Colarco *et al.* 2004; Müller *et al.* 2005). LiDAR emits laser beams and receives backscatter signals from smoke particles that can be processed to provide spatial and temporal variations of smoke concentrations. LiDAR has the advantage of simplicity, low cost, equipment mobility, robustness and low energy consumption (Lavrov *et al.* 2006) and is amenable to several platforms: ground, aircraft and satellite. Kovalev *et al.* (2009) stated that LiDAR was the most appropriate tool for ground-based monitoring of wildfire smoke plume dynamics and heights at different downwind distances. There are two satellites that are capable of defining plume injection height: the Cloud-Aerosol LiDAR with Orthogonal Polarisation (CALIOP) aboard the Cloud-Aerosol LiDAR and Infrared Pathfinder Satellite Observations (CALIPSO) satellite (Winker *et al.* 2006) and the Multi-angle Imaging Spectroradiometer (MISR) aboard the US National Aeronautics and Space Administration (NASA) Terra satellite (Kahn *et al.* 2007, 2008; Labonne *et al.* 2007; Diner *et al.* 2008; Raffuse *et al.* 2009; Amiridis *et al.* 2010). Although these satellites have global coverage, the temporal frequency is low (16 days for CALIOP and 9 days for MISR).

Smoke plume height model evaluation for prescribed fires is a challenge because of limited smoke plume height validation data (Jones and Christopher 2008). This makes it difficult to understand the performance and uncertainties of smoke models. Fire and smoke model validation is one of the fundamental research issues identified in the Smoke Science Plan (Riebau and Fox 2010), prepared for the US Joint Fire Science Program (JFSP). The JFSP and the Strategic Environmental Research and Development Program (SERDP) have supported several research projects to collect smoke data for model validation. This paper presents results from smoke plume rise measurements of prescribed fires in the south-eastern US.

Methods

Burn sites

Smoke plume height was measured at four sites in the south-eastern USA (Fig. 1), including the Fort Benning Army Base, Columbus, Georgia (32°33′N, 84°79′W), the Oconee National Forest, Eatonton, Georgia (33°54′N, 83°46′W), the Piedmont National Wildlife Refuge, Hillsboro, Georgia (near the Oconee National Forest), and Eglin Air Force Base, Niceville, Florida (30°32′N, 86°29′W). Fort Benning is located in the south-eastern plains ecoregion. Most of the upland area is considered sandhill and is managed for longleaf pine, with other areas of more clayey soils. Stands encompass scrub oak–pine, pine–hardwood and oak–hickory forest types. Fire management objectives are to maintain a maximum of rotation of 3 years (though in practice some areas may have longer rotation periods) while keeping
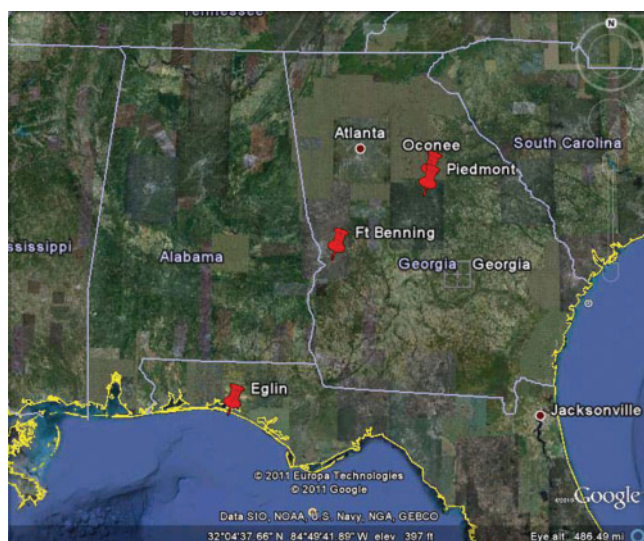
Fig. 1.   Location of the four burn sites at Fort Benning, Oconee, Piedmont and Eglin in south-eastern US, shown on Google Earth.

smoke within the confines of the military base. All burns are ground-ignition fires, conducted mostly during late winter and early spring.

The Oconee National Forest and the Piedmont National Wildlife Refuge are located in the Piedmont region of Georgia, which lies between the Atlantic Coastal Plain and the Blue Ridge Mountains. This region consists mostly of low hills and narrow valleys. The majority of the forests is mixed, consisting primarily of an overstorey of oak, hickory and pine. The National Forest and the Refuge also have extensive areas of almost pure upland pine maintained by fire. The Oconee National Forest plan is to burn between 4000 and 8000 ha year^{-1} (10 000 and 20 000 acres year^{-1}) on a 3–5-year rotation. Because of the high fire return frequency, fuel loading is generally light and produces slow-burning fires with low flame heights. The area, stand types and ignition methods vary depending on land-management objectives. Therefore, fire behaviour also varies. Large-area burns are usually conducted by backing fires through ground ignition to create black lines, followed by aerial ignition.

Eglin Air Force Base is located in the East Gulf Coastal Plain ecoregion. A majority of habitats are fire dependent and maintained by one of the largest fire-management programs in the country. Most of the area is a sandhill ecosystem, which consists of longleaf pine overstorey. The management goal of the prescribed-fire program requires burning large tracts through aerial ignition.

Detection device

Smoke plume height was measured with the Vaisala CL31 ceilometer (Helsinki, Finland) (Münkel *et al.* 2007) (Fig. 2*a*) designed using laser LiDAR technology. It emits short, powerful laser pulses in a vertical or slant direction, operating at a wavelength of 0.9 μm and is thus sensitive to the fine particulate matter (PM) found in smoke plumes. The directly backscattered light from smoke particles is measured as the laser scans the sky.
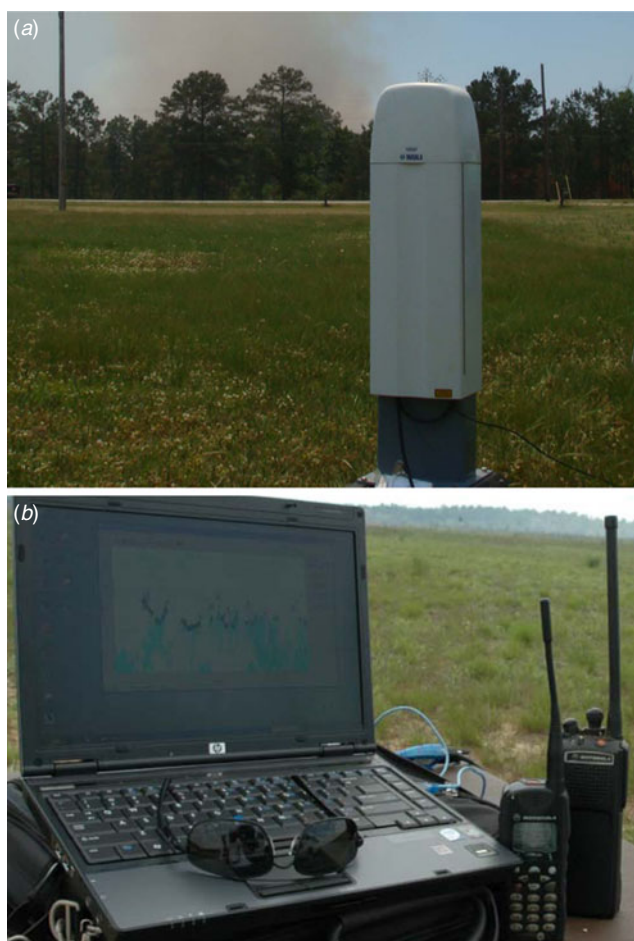

Fig. 2.   CL31 ceilometer with smoke plume in the background (*a*) and automated storage and display on a PC (*b*).

This is an elastic backscatter system and the return signal is measured at the same wavelength as the transmitted beams. As many as three smoke layers can be detected with the height up to 7.5 km at a resolution of 20 m. The detection frequency is as high as 2 s. The ceilometer is connected to a PC computer for automated data storage and display (Fig. 2*b*). An application (CL-VIEW) is used to visualise the data for monitoring operation of the ceilometer during the measurement period. Depending on weather conditions and burn intensity, in this study the ceilometer was located 3–10 km downwind from the burn and pointed vertically. In a few cases the actual wind directions were outside the predicted range, leading to relocation of the ceilometer shortly after the burning had started.

Although originally designed to determine cloud heights, ceilometers have been used for detecting air pollutants and planetary boundary layer (PBL) structure in recent years (McKendry *et al.* 2010). Tsaknakis *et al.* (2011) compared a CL31 ceilometer with two other types of LiDAR in Athens, Greece, under various strongly different aerosol loads or types (urban air pollution, biomass burning and Saharan dust event). In general, good agreement was found between the ceilometer and other instruments in detecting the mixing layer height, PBL structure and tropospheric aerosol vertical profiles

Tsai *et al.* (2009) measured a prescribed burn at Fort Benning in 2008 using a CL31 ceilometer and a millimetre-wavelength Doppler radar. Similar plume morphology existed in both measurements; but the LiDAR backscatter was strongly attenuated above 1 km and the radar echo extended higher than the LiDAR signals. The laser light source used in ceilometers is less powerful and spectrally broader than that of the radar; thus the ability of ceilometers to detect aerosols is restricted to 3-km height or less (Markowicz *et al.* 2008).

Smoke concentration

$PM_{2.5}$ and PM_{10} concentrations were estimated from backscatter using the following formula (Münkel *et al.* 2004, 2007):

$$C_{PM_{10}} = m\beta + b \qquad (1)$$

$$C_{PM_{2.5}} = 0.6846 + 0.8608 \times C_{PM_{10}} \qquad (2)$$

where $C_{PM_{2.5}}$ and $C_{PM_{10}}$ are $PM_{2.5}$ and PM_{10} concentrations, β is the measured smoke backscatter coefficient and regression coefficients are $m = 2.023 \times 10^7\,\mu g\,m^{-2}$ srad (solar radiation) and $b = -1.6304\,\mu g\,m^{-3}$.

Note that these formulae were obtained based on backscatter data measured with a CT25KA ceilometer (a Vaisala ceilometer older than that used in the present work). Further studies incorporating a CL31 ceilometer for refinement and finalisation of this formula are required (Münkel *et al.* 2007). Furthermore, the formulae were developed based on the measurements of pollutants at a low elevation (20 m above the ceilometer location). Possible uncertainties in their applications to fire smoke plumes at much higher elevations are yet to be determined.

Wavelet transform

Wavelet transform was used to analyse temporal fluctuations of the measured smoke plume height. Smoke plumes rise in the PBL, where turbulent motions often make it difficult to identify temporal variability in smoke plume height. Spectral or signal analysis techniques are needed to extract the variability. Similar to the Fourier transform, the wavelet transform, introduced by Morlet *et al.* (1982*a*, 1982*b*), is a tool to extract cyclic information (various spectrum or scales, amplitude and phase) hidden in a series, or to represent the series with certain-degree filtering. However, unlike the Fourier transform, the wavelet transform is conducted in a scale-location domain (the location can be either space or time), enabling one to identify not only various scales and amplitudes but occurrences of abrupt events with a certain scale. In addition, scale-location resolution is dependent on the scale parameter. These properties are especially useful for analysing motion in the PBL, which is nonstationary, nonlinear and characterised by a variable temporal domain. Because of these unique properties, the wavelet transforms have been widely used for theoretical analysis and practical application (e.g. Meyer 1993; Liu 2005).

The wavelet transform of a time series ($f(t)$) is defined as:

$$Wf(\lambda, t) = \int_{-\infty}^{\infty} f(u)\psi_{\lambda,t}(u)\,du \qquad (3)$$

$$\psi_{\lambda,t}(u) \equiv \frac{1}{\sqrt{\lambda}}\psi\left(\frac{u-t}{\lambda}\right) \qquad (4)$$

where $\lambda\,(>0)$ is a scale parameter, t a location parameter and the function $\psi_{\lambda,t}(u)$ wavelet with the properties of zero mean and normalisation. The wavelet variance (also called energy), integration of module of the wavelet transform over entire locations, gives a measure of relative contribution of a specific scale to total variance:

$$E(\lambda) = \int_{-\infty}^{\infty} |Wf(\lambda, t)|^2\,dt \qquad (5)$$

In this study, the Morlet wavelet (Morlet *et al.* 1982*a*):

$$\psi(u) = \pi^{-1/4}e^{-i\omega}ue^{-u^2} \qquad (6)$$

was adopted, where ω_o was specified with the value of 5.

For practical applications, the integration with Eqn 3 or Eqn 5 was approximated by summation with discrete parameters λ and t. Range of the summation is $l \pm n/2$, where $l = t$ or u and n is an even integer number and not greater than the sample of the series. Notice that the limited sample in a discrete series would generate edge effects in the calculation of larger scales so that scale information at the edges of the series may be unrealistic. Thus, caution should be taken regarding large scales such as those having full or half length of the analysed series. When analysing the time dependence of scales, some wavelet transform values close to the two ends of the location component of the scale-location domain are often excluded; the longer a scale, the larger the number (Torrence and Compo 1998).

Results

Prescribed burns

A total of 20 prescribed burns were measured between 2009 and 2011 (Table 1); six at Fort Benning (named as F1–F6 hereafter for convenient description), five at Oconee (O1–O5), one at Piedmont (P1) and eight at Eglin (E1–E8). Five burns were in winter, thirteen in spring and two in summer. Burned areas were: less than 202 ha (500 acres) for four burns, 202–404 ha (500–999 acres) for six burns, 405–808 ha (1000–1999 acres) for eight burns and 809 ha (2000 acres) or larger for two burns. Ground ignition was used for all burns at Fort Benning and two burns at Eglin AFB. Aerial ignition was used for all burns at Oconee NF and Piedmont NWR and for five burns at Eglin AFB. Fig. 3 shows images of the 20 burns. Smoke plumes were well developed for burns F1, F6, O1, E3–E6 and E8. The sky was mostly clear for 14 burns, partly cloudy for 3 burns (O4, E3 and E4) and mostly cloudy for 3 burns (O1, O2 and P1).

Smoke plume height

Figs 4–6 show the time-vertical cross-sections of backscatter from the prescribed burns. The colours indicate intensity of backscatter signals, which are proportional to smoke concentrations. It can be seen that the backscatter signals at a specific time were visible and continuous until a certain elevation, which is the height for smoke plume height, cloud base or the PBL. Backscatter signals for smoke plumes usually distributed continuously within a layer from the ground to the elevation and varied with time in their intensity. In contrast, backscatter signals for clouds usually distributed only within a narrow vertical

Table 1.   Prescribed burn information

Burn site	Number	Name	Date	Area burned (ha) (acres)	Ignition
Fort Benning	1	F1	14-Jan-09	147.3 (364)	strip head
	2	F2	15-Jan-09	235.9 (583)	strip head
	3	F3	4-Aug-09	95.5 (236)	strip head
	4	F4	4-Sep-09	138.8 (343)	strip head
	5	F5	28-Apr-10	404.7 (1000)	strip head
	6	F6	29-Apr-10	180.9 (447)	strip head
Oconee	7	O1	24-Mar-09	639.4 (1580)	aerial
	8	O2	25-Mar-10	1011.7 (2500)	aerial
	9	O3	4-Jan-10	293.4 (725)	aerial
	10	O4	4-Feb-10	432.6 (1069)	aerial
	11	O5	4-Jul-10	403.1 (996)	aerial
Piedmont	12	P1	27-Apr-09	483.6 (1195)	aerial
Eglin	13	E1	5-Jun-09	202.3 (500)	strip head
	14	E2	5-Jul-09	259.4 (641)	strip head
	15	E3	5-Aug-09	428.2 (1058)	aerial
	16	E4	6-Jun-09	607.0 (1500)	aerial
	17	E5	6-Jul-09	647.5 (1600)	aerial
	18	E6	2-Jun-11	667.7 (1650)	aerial
	19	E7	2-Aug-11	828.0 (2046)	aerial
	20	E8	2-Dec-11	202.3 (500)	strip head

layer around an elevation and maintained mostly constant intensity with time. Backscatter signals for the PBL were usually very weak. For burn O2, for example, weak backscatter signals were visible within ~500 m above ground during the first hour of the measurement period, whereas slightly more intense signals were visible within ~200 m above ground. The elevations of 500 and 200 m were considered as the PBL and smoke plume heights. Intense signals were seen above 500 m after that time and even more intense signals occurred at ~1500 m above ground, within a layer ~100 m deep. The elevations of 500 and 1500 m were considered as smoke plume height and cloud base.

Fig. 7 shows the mean of the smoke plume height over the entire measurement period for each burn. The mean is also listed in Table 2. The average of the smoke plume height means for all burns was slightly above 1 km. Smoke plume heights varied considerably among the burns and depended on the season of burn occurrence. Smoke plume heights at Fort Benning for the two burns in mid-January were ~0.75 and 0.65 km; they increased to 0.8–0.9 km for the next two burns in early April and further increased to nearly 1.2 km for the last two burns in late April. Smoke plume height is proportional to heat energy released from fire and atmospheric instability, so burns of larger area produce more energy and warmer atmosphere tends to increase instability. In this case the last two burns had larger burned areas and occurred during warmer atmospheric conditions.

Smoke plume heights were between ~1.05 and 1.2 km for the five burns at Oconee NF in late March and early April, and nearly 1.3 km for the burn at the nearby Piedmont NWR in late April.

The values at Eglin AFB were between 0.95 and 1 km for the first three burns in spring; they increased to ~1.1 and 1.25 km for the next two burns in early summer and then decreased to ~0.9 and ~1 km for the last three burns in late winter. Little difference appeared at this location between the spring

and winter seasons. A possible explanation is that, in spite of cooler conditions, the burns in early February either had larger burned areas or aerial ignition was used.

The averaged smoke plume height was 842 m for the five winter burns, 1070 m for the thirteen spring burns and 1140 m for the two summer burns. Thus, smoke plume height showed an increasing trend from winter to summer.

Also shown with each mean value in the figure are minimum and maximum hourly values. Hourly values for a specific 1-h period (e.g. 1200–1300 local time) were obtained if smoke measurement during this period was longer than 10 min. Smoke plume height during a burn period can change substantially from one hour to the next. The difference between minimum and maximum hourly smoke plume heights was ~300 to 500 m for burns F1, F6, O1, O3–O3, P1, E1, E5–E6 and E8. The largest range was more than 1000 m for burn O2.

Table 3 lists smoke plume height and the corresponding fuel moisture (FM) and fire-danger rating (FDR) for each burn, obtained from the Remote Automatic Weather Stations (RAWS) (www.raws.fam.nwcg.gov/nfdrs/Weather_station_standards_rev08_2009_FINAL.pdf, accessed 19 March 2012) and the Wildfire Danger Assessment System (WFAS) (www.wfas.net/index.php/fire-danger-rating-fire-potential-danger-32, accessed 9 September 2012). The 10-h FM was ≤7.5% for burns F3–F3, O3–O5, P1 and E3–E5, >10% for burns F1–F2, E1 and E6–E7, and in between for other burns. The 100-h FM was 11–15% for all but one of the burns (16–20%) at Fort Benning, Oconee NF and Piedmont NWR, and 16–20% or greater for all burns at Eglin AFB. The 1000-h FM was greater than 20% for 16 burns and 16–20% for 4 burns. FDR were mostly moderate at Fort Benning (five out of six burns) and Oconee NF and Piedmont NWR (four out of six), and mostly low at Eglin AFB (seven out of eight).

A more detailed analysis of the effects of FM and FDR on plume height was done as follows. Smoke plume height values
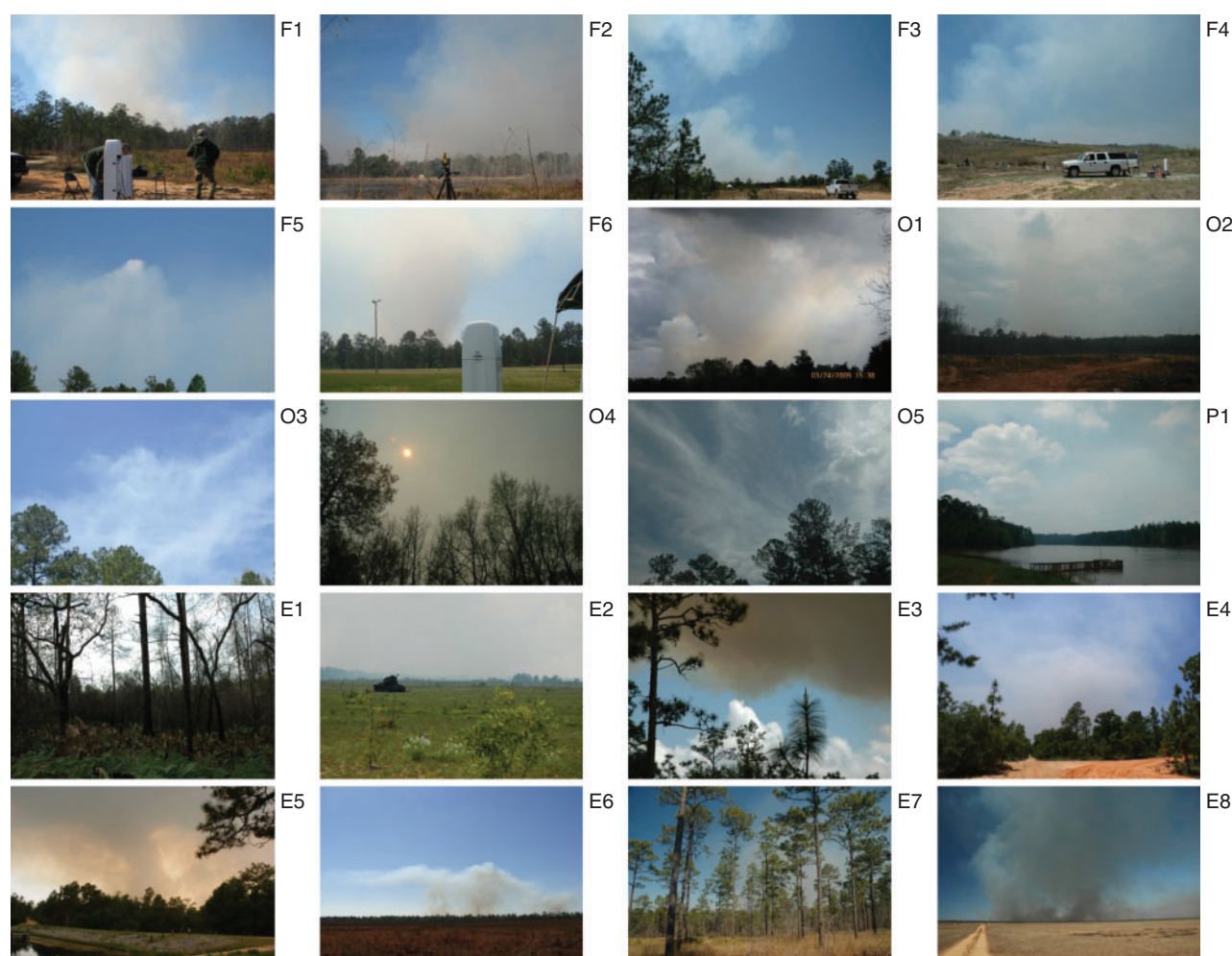
Fig. 3. Pictures of smoke plumes from the 20 prescribed burns in south-eastern US. The panel labels represent burn sites (F, Fort Benning; O, Oconee; P, Piedmont; E, Eglin) and burn number. See Table 1 for detailed burn information.

were divided into three categories of 'above' (plume height >1100), 'normal' (900–1100) and 'below' (<900 m). Accordingly, 10- and 100-h FM was divided into dry, normal and wet categories with the values of <7.5, 7.5–10 and >10% for 10-h FM and 11–15, 16–20 and >20% for 100-h FM. Because FDR and 1000-h FM each had only two values or ranges, they were divided into dry and wet categories with the values of 16–20 and >20% for 1000-h FM and moderate and low for FDR. For 10-h FM, 13 burns had above, normal and below smoke plume heights *v.* dry, normal and wet FW; 1 burn had below plume height *v.* dry FM; and 6 burns had above or below plume heights *v.* normal FS or normal plume heights *v.* dry or wet FM. The corresponding numbers of burns for 100-h FM for the three situations were eight, five and seven. The 1000-h FM had above, normal and below smoke plume heights *v.* dry, normal and wet FW for five burns, and above and below plume height *v.* wet and dry FM for seven burns. The corresponding numbers for FDR were four and eight. The burns with normal plume heights were not compared for 1000-h FM and FDR It is apparent that 10-h fuel moisture had a much bigger effect on smoke plume height than did 100- and 1000-h FM and FDR.

Smoke plume intensity

Smoke plume intensity was measured by $PM_{2.5}$ and PM_{10} concentrations calculated from backscatter signals. $PM_{2.5}$ and PM_{10} means for a burn were obtained over the vertical-temporal section within the smoke plume where the concentrations were greater than $20\,\mu g\,m^{-3}$, the assumed background level of pollutants. The averages of $PM_{2.5}$ and PM_{10} means for all burns were 79 and $91\,\mu g\,m^{-3}$ (Fig. 8). Note that the concentrations usually showed a decreasing trend with downwind distance. The distance dependence, however, could not be quantitatively determined in this study because only one ceilometer was used. $PM_{2.5}$ and PM_{10} concentrations were 102.0 and $117.4\,\mu g\,m^{-3}$ for winter, 73.7 and $85.0\,\mu g\,m^{-3}$ for spring and 54.5 and $62.0\,\mu g\,m^{-3}$ for summer burns. Thus, on average the PM concentrations were the largest in winter and smallest in summer despite large inner-seasonal variability at some burn sites. One possible reason for this seasonal trend could be the increasing trend in plume height from winter to summer. The PM concentrations should be higher within lower height plumes (a case for winter on average) if other properties such as total emissions are the same.
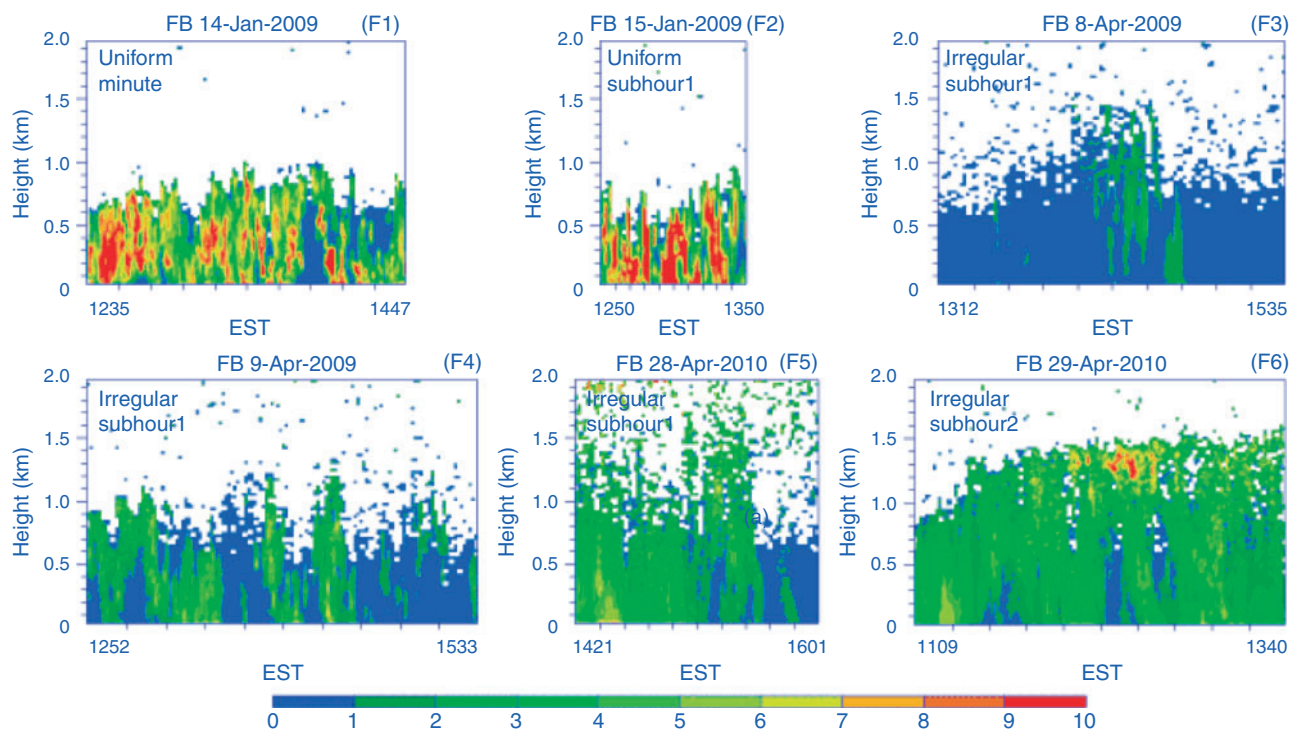
Fig. 4. Ceilometer backscatter signals (10^3 srad km^{-1}) for six burns at Fort Benning (F1–F6). The two numbers below each panel are start and end times (Eastern Standard Time, EST) of the smoke measurement period. The backscatter intensity (equivalent to PM concentrations) is indicated by the colours. The burn site and date are shown on top of each panel. Descriptors of the fluctuation pattern and major scale range are given within each panel.

Temporal variability patterns

Smoke plume height and PM concentrations were continuously dynamic, as shown in Fig. 9. The three burns shown in the figure each represent a temporal variation pattern. The first pattern (uniform) is characterised by fast and uniform temporal fluctuations. Smoke plume height for burn E2 (Fig. 9a) was mostly within ~0.2 km of a height of 0.9 km. Smoke plume heights for burns F1, F2, E1 and E3 also showed the uniform fluctuation pattern.

A second pattern (irregular) was characterised by slow and irregular fluctuations in plume height. Smoke plume height for burn E5 (Fig. 9b) was between ~1.2 and 1.7 km in the first hour of the measurement period, oscillated at ~1 km in the following 3 h or so, and increased to more than 1.2 km in the final hour. Other plumes with this behaviour were F3–F6, O3–O5, E4, E5, E7 and E8. Fast fluctuations were superimposed on irregular fluctuations for many burns, especially F4 and F5.

A third pattern (capped) was characterised by a temperature inversion layer (clear-sky cap) or cloud (cloudy-sky cap) just above the smoke plumes. Burn E6 (Fig. 9c) was a clear-sky-cap case. As seen in Fig. 3 (E6), the vertically well-developed smoke plumes drifted horizontally when they reached a certain altitude. The corresponding smoke plume height gradually decreased from ~1.2 to 0.8 km (Fig. 9c). Burn O1 was a cloudy-sky-cap case, with clouds shown in Fig. 3 (O1). The height of clouds gradually increased from ~0.9 to 1.3 km during the first 3 h of the measurement period; the smoke plume height was ~0.8 km in the first hour and then increased to the cloud height. O2 and P1 were two other burns showing the capped pattern. An increasing

or decreasing trend was accompanied by uniform or irregular fluctuation patterns or both.

Variation in the height of the largest PM concentration followed the variation in smoke plume height for all burns. The distance between the height of largest PM concentration and the smoke plume height was mostly constant for the uniform pattern (Fig. 9a). For the irregular fluctuation pattern, the distance was very small in the first half of the measurement period but increased in the second half (Fig. 9b). For the capped pattern the distance was sometimes large during the measurement period (Fig. 9c).

Timescales of fluctuations

Wavelet variances of individual scales in temporal variability of smoke plume height are shown in Fig. 10. The values are normalised by the sum of the variances of all scales. The timescale in the wavelet transform measures frequency of fluctuation; the shorter a scale, the faster the fluctuation. Wavelet power (variance) measures intensity of a scale. All scales (t, h) are grouped into four ranges based on the intensity of the major scales, which are defined here as the scales with normalised variances greater than 10%: $t < 0.25$ (short range), $0.25 \leq t < 2$ (intermediate), $2 \leq t < 4$ (long) and $t \geq 4$ (extra-long).

For burns F1, E1–E3 and E6, (Fig. 10a), no major scales were found in the short range or other ranges (in fact, no major scales were found in the short range for any burn). The ratio of the sum of variances of all scales in a range, to the sum of variances of all scales in all ranges, is shown in Fig. 11. The ratios for these burns were ~22–40% for the short range, compared with ~28–46%
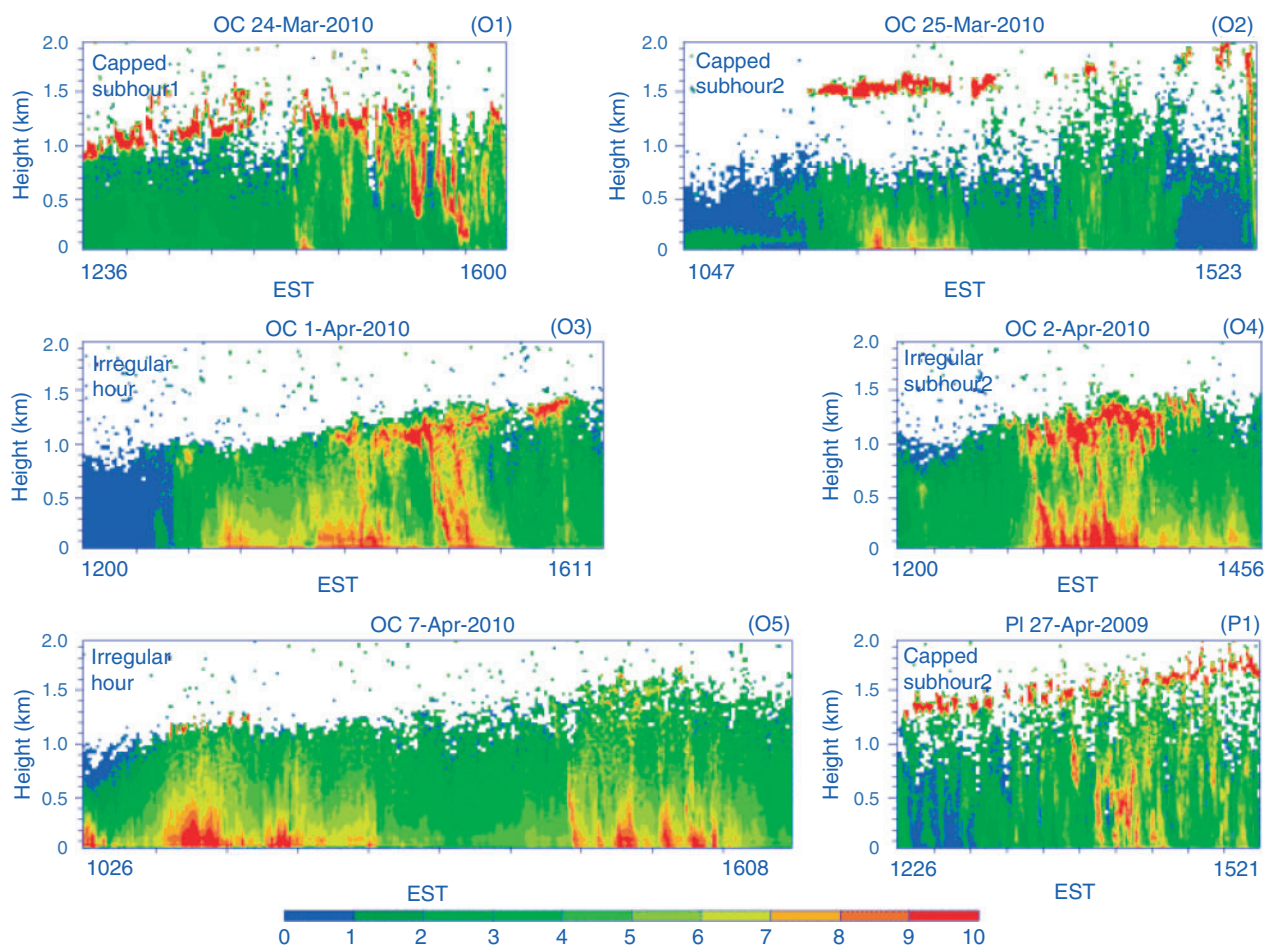
Fig. 5. Ceilometer backscatter signals (10^3 srad km^{-1}) for six burns at Oconee (O1–O5) and Piedmont (P1). Figure labels are as per Fig. 4.

for the intermediate range, 21–32% for the long range and 0–17% for the extra-long range (Fig. 11*a*). Thus, the contributions to plume height fluctuations from the scales in the short range were comparable to those from the scales in the other ranges for these burns.

Burns F2–F5, O1, E4 and E7 had major scales only in the intermediate range (Fig. 10*b*) with ratios of ~50–75% (Fig. 11*b*). The ratios of scales in the short range were also large (~18–42%) for burns F2, F4 and F5. Burns F6, O2, O4, P1 and E8 had major scales only in the long range (Fig. 10*c*) with ratios of ~35–57% (Fig. 11*c*). Burns O3, O5 and E5 had major scales only in the extra-long range (Fig. 10*d*) with ratios of ~33–70% (Fig. 11*d*).

It can be seen from Table 2 and Figs 4–6 that four out of five burns with the uniform fluctuation smoke pattern (F1, E1–E3) had major scales in the short scale range. For the only exception (F2) that had major scales in the long range, contributions from scales in the short range were also noticeable. The burns with the irregular smoke pattern had major scales in the intermediate (burns F3–F5, E4 and E7), long (F6, O4 and E8) and extra-long (O3, O5 and E5) ranges. The burns with the capped-smoke pattern had major scales in the short (burn E6), intermediate (O1) and long (O2 and P1) ranges.

For a specific burn with major scales in a certain range, the scales may be noticeable only in certain time stretches during the measurement period. Fig. 12 shows variations of wavelet variance with time of measurement for burn E5. The vertical coordinate indicates timescales of smoke plume height fluctuation, and the horizontal coordinate indicates the time of measurement. The colours indicate wavelet power (variance) of various scales with increasing intensity signals from blue to purple. Fast fluctuations were more remarkable in the first few hours of the measurement period, as indicated by large variances during the time periods between ~1200 and 1500 hours Eastern Standard Time (EST) for the scale of ~4 min, 1400 and 1500 hours EST for the scale of ~8 min and between 1230 to 1315 and 1430 to 1445 hours EST for the scales of 20 and 30 min. In contrast, slow fluctuations at the scales of 1–2 and 4 h were noticeable throughout the measurement period.

Vertical distribution of backscatter signals

Fig. 13 shows vertical profiles of smoke backscatter averaged over every half hour during the measurement periods for the three burns representing different fluctuation patterns. For the uniform pattern (E2), vertical profiles were similar among all time periods except the last. The backscatter values were almost
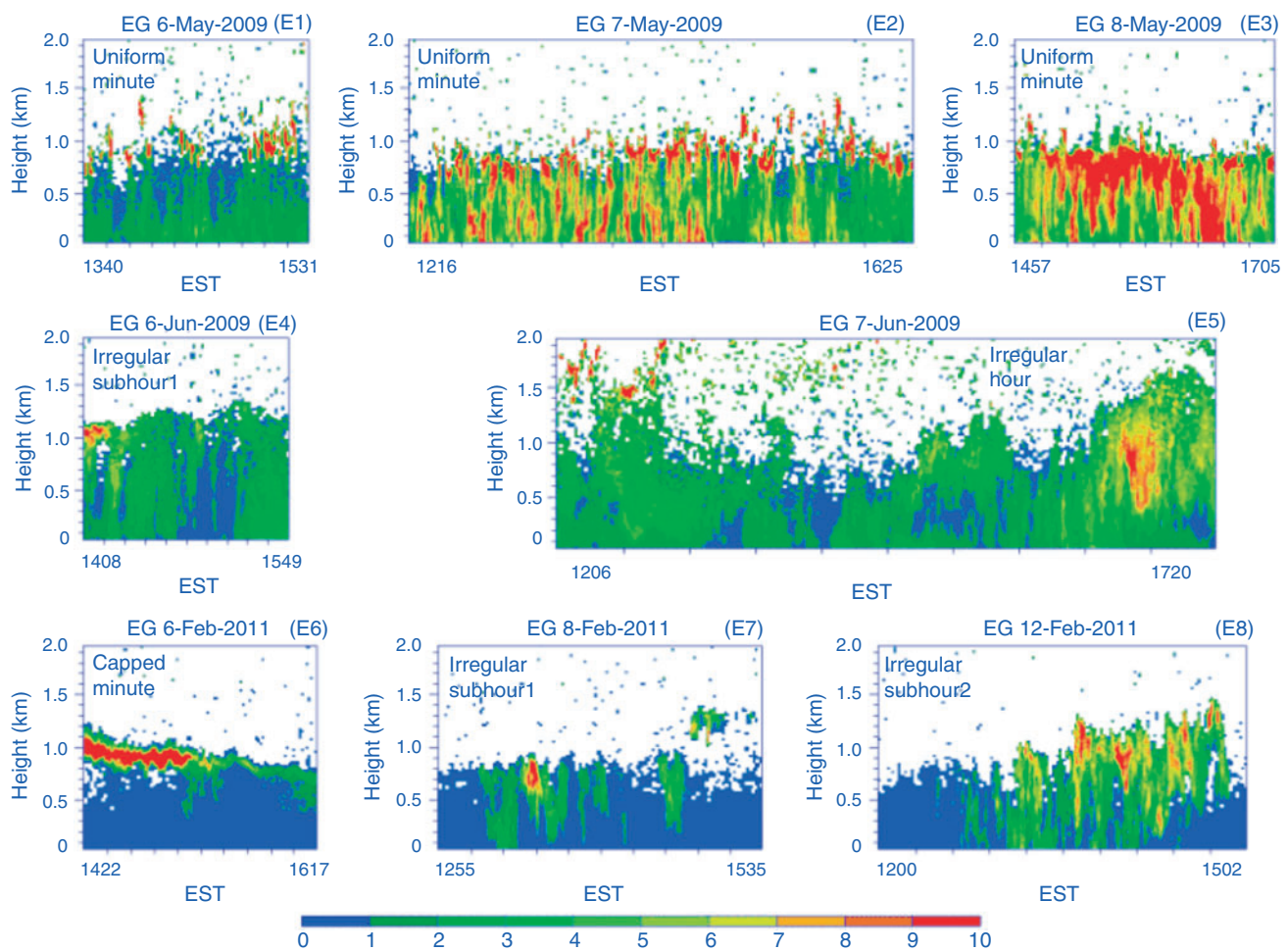
Fig. 6. Ceilometer backscatter signals (10^3 srad km^{-1}) for eight burns at Eglin (E1–E8). Figure labels are as per Fig. 4.
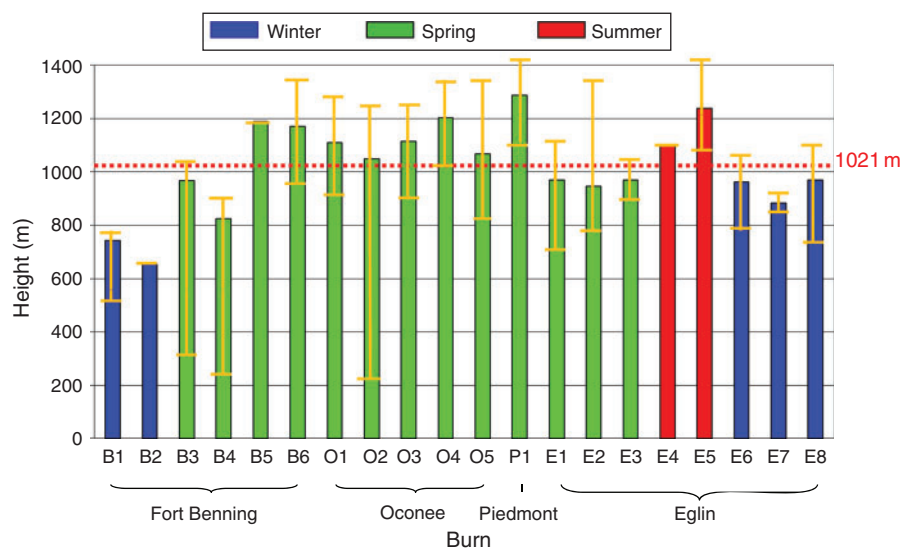

Fig. 7. Smoke plume height means (bars) and ranges between minimum and maximum hourly values (yellow lines) for each burn. The dotted line is average smoke plume height of all burns. See Table 1 for burn names.

Table 2. Measured smoke properties of prescribed burns

H_{ave}, H_{min} and H_{max} are mean, minimum and maximum hourly smoke plume heights. H_{conc} is the height at which the largest PM concentrations were detected. The 'pattern' column denotes smoke plume height fluctuation pattern over time. PM values are in micrograms per cubic metre

Burn	H_{ave}	H_{min}	H_{max}	H_{conc}	PM$_{2.5}$	PM$_{10}$	Pattern	Scale range
F1	744	496	759	312	105	121	uniform	short
F2	655	644	644	265	156	181	uniform	intermediate
F3	967	277	1033	761	43	50	irregular	intermediate
F4	825	206	839	517	56	65	irregular	intermediate
F5	1189	1187	1192	958	57	66	irregular	intermediate
F6	1170	982	1350	944	58	66	irregular	long
O1	1110	909	1265	944	72	83	capped	intermediate
O2	1050	206	1250	863	62	72	capped	long
O3	1115	918	1256	582	86	99	irregular	extra long
O4	1203	1019	1320	699	89	103	irregular	long
O5	1067	813	1364	575	84	97	irregular	extra long
P1	1287	1118	1429	1080	80	92	capped	long
E1	970	695	1106	740	50	58	uniform	short
E2	946	809	1334	666	96	110	uniform	short
E3	970	892	1030	662	125	144	uniform	short
E4	1102	1088	1115	886	47	53	irregular	intermediate
E5	1238	1102	1460	1015	62	71	irregular	extra long
E6	962	793	1047	848	127	146	capped	short
E7	882	849	895	673	51	58	irregular	intermediate
E8	969	730	1122	750	71	81	irregular	long

Table 3. Fire weather information, including 10-, 100- and 1000-h fuel moisture (FM$_{10}$, FM$_{100}$ and FM$_{1000}$, %) and fire danger rating (FDR)

H_{ave} is mean hourly smoke plume height. Δ represents categories (see text for definitions)

Burn	H_{ave}		FM$_{10}$		FM$_{100}$		FM$_{1000}$		FDR
	Value	Δ	Value	Δ	Value	Δ	Value	Δ	Rate
F1	744	below	11.99	wet	11–15	wet	>20	dry	moderate
F2	655	below	11.13	wet	11–15	wet	>20	dry	moderate
F3	967	normal	7.50	wet	11–15	wet	>20	dry	moderate
F4	825	below	7.48	dry	11–15	wet	>20	dry	low
F5	1189	above	7.21	dry	11–15	wet	16–20	wet	moderate
F6	1170	above	8.55	normal	11–15	wet	16–20	wet	moderate
O1	1110	above	8.84	normal	11–15	wet	>20	dry	moderate
O2	1050	below	9.29	normal	16–20	normal	>20	dry	low
O3	1115	above	5.83	dry	11–15	wet	>20	dry	moderate
O4	1203	above	6.20	dry	11–15	wet	>20	dry	low
O5	1067	normal	7.48	normal	11–15	wet	16–20	wet	moderate
P1	1287	above	6.45	dry	11–15	wet	16–20	wet	moderate
E1	970	below	12.03	wet	16–20	normal	>20	dry	low
E2	946	normal	8.71	normal	16–20	normal	>20	dry	low
E3	970	normal	7.27	dry	16–20	normal	>20	dry	low
E4	1102	above	7.35	dry	16–20	normal	>20	dry	low
E5	1238	above	6.75	dry	16–20	normal	>20	dry	moderate
E6	962	normal	13.40	wet	>20	dry	>20	dry	low
E7	882	below	11.20	wet	>20	dry	>20	dry	low
E8	969	normal	9.13	normal	16–20	normal	>20	dry	low

constant from the ground to a certain height where they gradually decreased towards the top of the smoke plume. Backscatter at a height of 0.8 km is very large during the last time period. This was most likely related to a new and intense ignition during the strip lighting process, although a definitive explanation cannot be provided without knowledge of the actual ignition time and fire intensity. For the irregular pattern (E5), large backscatter signals first occured in the lower portion of the smoke plume, but later moved to the upper portion. For the capped pattern (E6), large backscatter signals were found near the top of the smoke plume.

Among the 20 burns, large backscatter signals occurred mostly in the upper portion of smoke plumes for 8 burns, and the lower, for 3 burns, but did not change much vertically within
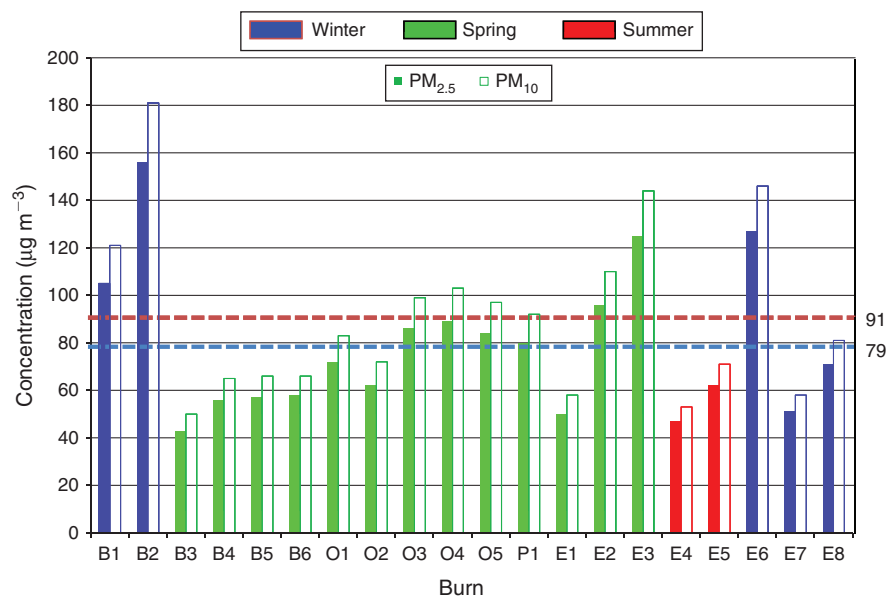
Fig. 8. $PM_{2.5}$ and PM_{10} concentrations of smoke plume averaged over measurement period for each burn. The light blue and brown dashed lines are $PM_{2.5}$ and PM_{10} averages of all burns. See Table 1 for burn names.
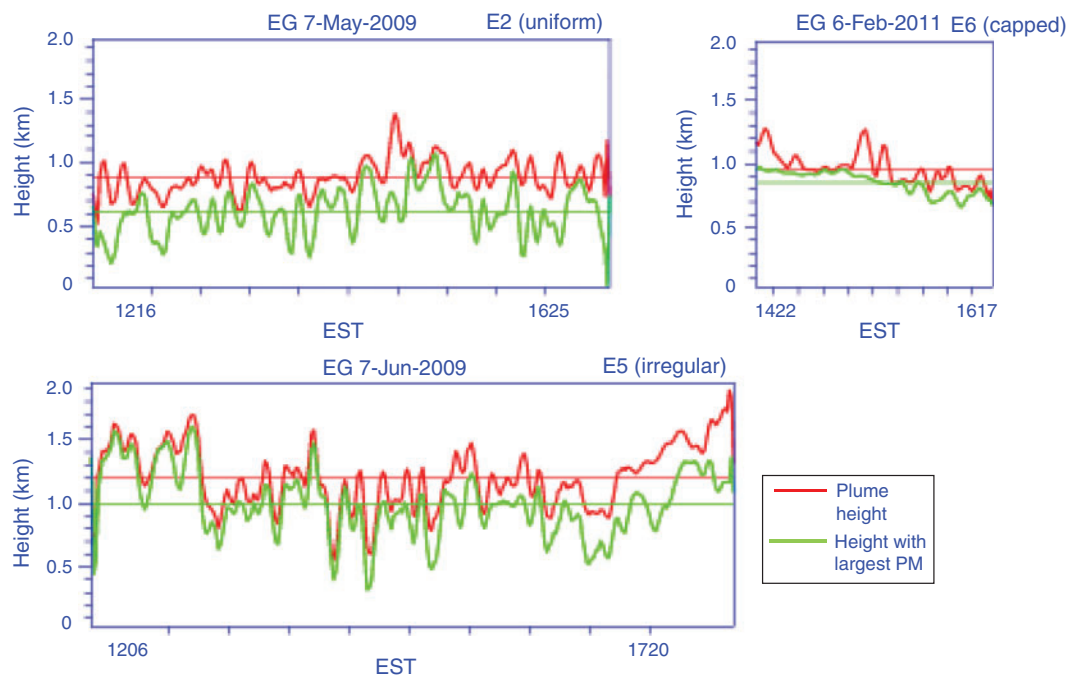

Fig. 9. Time series of smoke plume height for burns E2, E5 and E6, which have uniform, irregular and capped patterns of fluctuation. The red and green lines represent plume height and the height where the largest PM concentrations are located. The numbers below each panel are start and end times of the measurement period (Eastern Standard Time, EST).

smoke plumes for the remaining 9 burns. Vertical distribution of the density of a smoke plume is another important property required by CMAQ in addition to plume height for smoke and air-quality modelling. Because wind speed generally increases with height, a smoke plume with maximum concentration residing in its lower portion will have a smaller chance to affect air quality downwind. In addition, it is more difficult to simulate dispersion and transport of smoke particles in the lower portion of a smoke plume because of the effect of interaction with the surface, including tree canopy.

The measured vertical distribution of smoke provides useful data for evaluation of smoke models such as Daysmoke in simulating this feature.

Smoke plume and cloud

Previous studies have indicated the possible role of smoke in the formation or intensification of clouds and dense fog (e.g. Radke *et al.* 2001; Potter 2005; Achtemeier 2009). The related physical mechanisms include water released from fuel to the air during burning and air mass lifting due to heat energy released from fire and the creation of condensation nucleii. Cloud formation probably related to smoke plume was observed during two burns

in this study. Fig. 3 is a picture of one burn case (F5) that shows this phenomenon.

Discussion

Smoke plume height

Hardy *et al.* (1993) measured 23 prescribed fires of forest slash in the Pacific Northwest of the United States. They measured maximum plume heights, plume range, fuel mix, burning protocols, power output and atmospheric stability. The maximum plume heights were estimated visually by observers in light aircraft. The averaged maximum plume height of the 15 burns
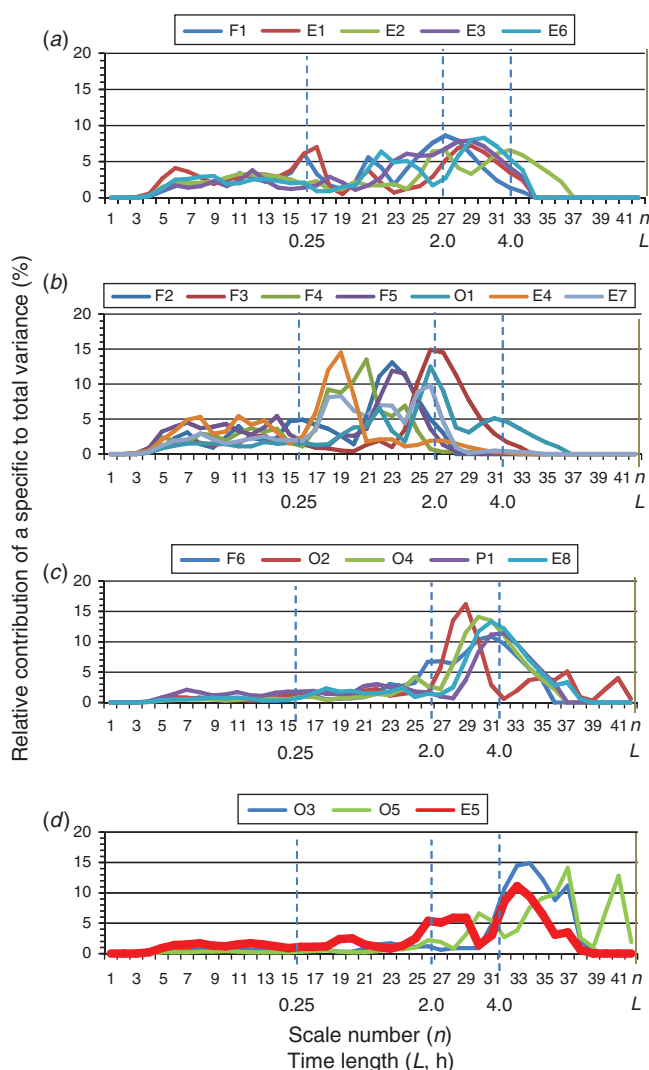

Fig. 10. Wavelet variances of smoke plume height fluctuations. The horizontal axes are scale number (n) and the corresponding scale length (L, h). The vertical dashed lines indicate the scales at 0.25, 2 and 4 h. The vertical axis is wavelet variance of individual scales normalised by the total variance of all scales (%). Panel (*a*) includes the burns with comparable wavelet variances from scales in all ranges. Panels (*b–d*) include the burns with major variance contributions from the scales in the intermediate, long and extra-long ranges. The heavy red line in panel (*d*) is the burn to be analysed for time dependence of scales shown in Fig. 12.
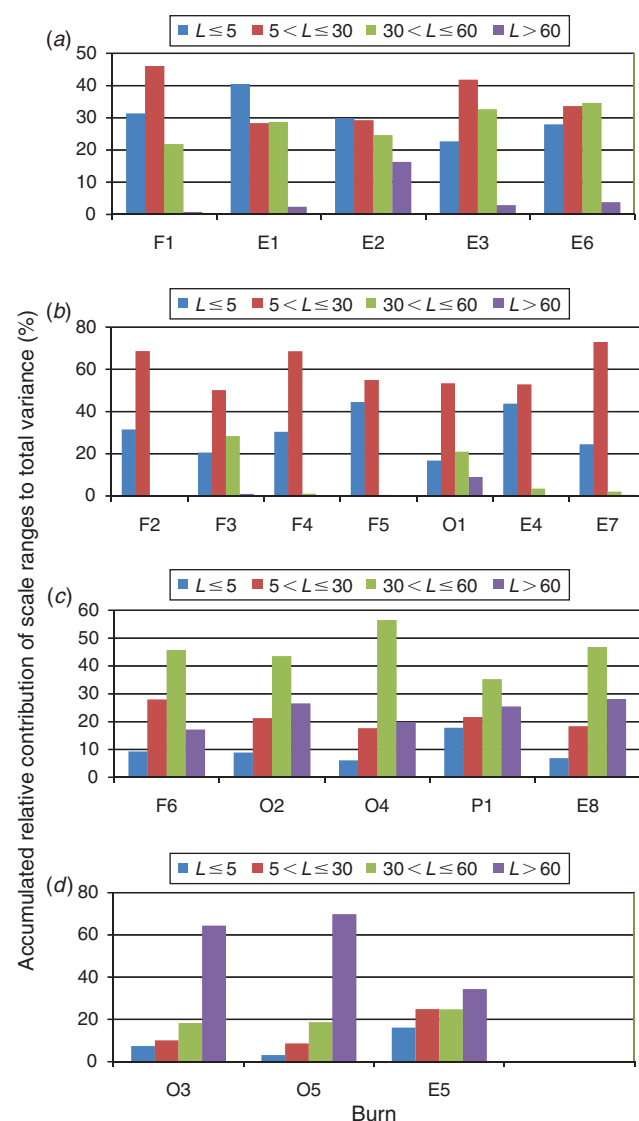
Fig. 11. Ratios of the sum of wavelet variances for scales within each range to the sum of wavelet variances for scales within all ranges. The bars represent the short (blue), intermediate (brown), long (green) and extra-long (purple) ranges. The horizontal and vertical axes are the burn and the ratio. Panel (*a*) includes the burns with comparable variance contributions from scales in all ranges. Panels (*b–d*) include the burns with major variance contributions from scales in the intermediate, long and extra-long ranges.

with substantially complete observations was ∼1.8 km (Harrison and Hardy 2002). Although this value is much larger than the average height of ∼1.0 km obtained in the current study, smoke plume heights from both studies are mostly within the PBL. There are several possible contributors to the differences between the two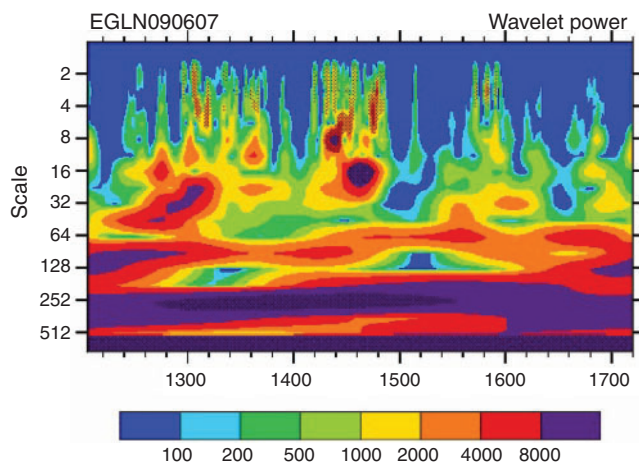 measurement studies. First, the previous study measured maximum plume height during the flight period whereas the present study gives average plume height over the entire measured period. Second, all burns for the previous study occurred during the summer whereas all burns except two for the current study are in winter and spring. Third, the fuel loads were considerably different as dead forest slash generally is drier and has much higher loading than did the fuels of the present study. Following Anderson (1982), slash fuel beds average ∼85 t ha^{-1} (∼34 tons acre^{-1}) of fuel whereas grass, shrub and litter fuel beds average ∼7.5, 20 and 17.5 t ha^{-1} (∼3, 8 and 7 tons acre^{-1}) (average fuel loadings include live fuel and dead fuel <7.5 cm (<3 inches) in diameter). On average a slash burn will consume more fuel and therefore release more heat than a typical eastern prescribed fire, which will result in a higher plume height. Fourth, all burns for the previous study were in areas with complex terrain whereas the burns of the present study were in fairly flat terrain. As described in Harrison and Hardy (2002), the burn sites of their study were predominantly located on the lateral slopes of alpine river valleys, and prescribed slash-burns were commonly ignited in the late morning, with up-valley thermal winds that were locally amplified by heat release from the fires. Their plumes did not rise solely from thermal buoyancy, but were significantly accelerated by up-valley convergence of horizontal winds.

Plume height modelling schemes have been developed for various local and regional air quality models. These schemes have different physical considerations, some of which may fit both wildfire and prescribed burns whereas others may better fit
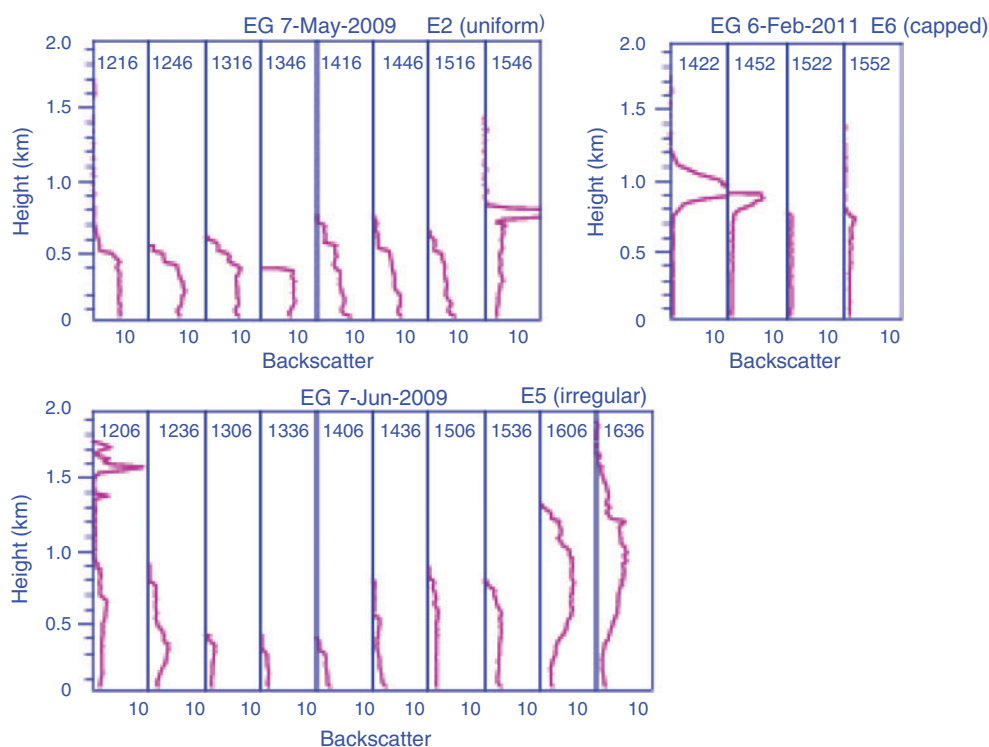

Fig. 12. Distribution of wavelet variance (m^2 s^{-2}) of smoke plume height for burn E5 (irregular fluctuation pattern). Vertical and horizontal axes are fluctuation scale (min) and time of measurement (Eastern Standard Time, EST). The colours from blue to purple indicate increasing intensity of wavelet power.

Fig. 13. Vertical profiles of backscatter signals. Panels E2, E5 and E6 are for the uniform, irregular and capped fluctuation patterns. The horizontal and vertical axes are backscatter signal (10^3 srad km^{-1}) and height (km). The boxes in each panel represent averages over every 30 min during the measurement period with the start time (Eastern Standard Time, EST) indicated in the upper portion of each box.

just one of these. Understanding the strengths and weaknesses of various schemes in modelling prescribed burn plume height can be improved through inter-comparing these schemes using the measured data from this study. Trentmann *et al.* (2002) used airborne remote sensing and *in situ* smoke plume measurements to compare the simulated dynamic evolution of a plume from a prescribed fire with the active tracer high-resolution atmospheric model. Previous investigations like Trentmann *et al.* (2002) have largely focussed on one burn or a very limited number of prescribed burns. The present study, however, measured a large number of burns; thus, the results can be used as systematic and statistical evaluation data for prescribed-burn model performance.

The measurements could be used to evaluate the capacity of smoke models in simulating the plume features observed in this study, including fluctuations at different timescales, and different types of vertical profiles and particulate matter concentrations. The fluctuation and varied vertical distribution features are related to fuels and ecosystem types, fire emissions and heat-energy release, atmospheric turbulence and eddy motions, and other complex dynamic and thermal processes. Thus, it is difficult for smoke models to reproduce these features. Evaluations would provide useful information to improve the description of these processes in smoke models. Unfortunately no meteorological data (profiles or surface values of wind speed and direction, temperature and turbulence) were collected during this study. These data are key determinants in plume rise and inputs in plume height models. Therefore the use of this dataset for the evaluation of plume height models for these types of buoyant sources is limited.

The measured smoke plume height could also be used to help estimate smoke plume parameters such as updraft core number (used in Daysmoke). Multiple updraft cores are smoke 'sub-plumes' and are the outcome of multiple ignitions, smoke plume interactions, heterogeneous distributions of fuels and other processes. Sub-plumes may initially rise separately and later merge into a single plume. The buoyancy created by multiple updraft cores is smaller than that generated by one single updraft core with a size equivalent to the integrated size of all updraft cores. The corresponding plume height is therefore smaller. The core number is one of the most important parameters in Daysmoke for plume height calculation (Liu *et al.* 2010; Achtemeier *et al.* 2011). However, this parameter is typically unavailable. Detection techniques and calculation schemes are yet to be developed. Achtemeier *et al.* (2011) found that Daysmoke obeys the 2/3 law for plume rise, similar to the Briggs plume rise scheme (Briggs 1975), for most plumes. The factors in smoke plume rise include heat flux, wind speed and entrainment coefficient; heat flux is determined by updraft core number, exit temperature and velocity, and burned area. Using the plume height measurements from this study, updraft core number could be retrieved if other parameters are known. However, this work is beyond this study because measurements and modelling of fuel, fire behaviour, and meteorology are needed to obtain these parameters.

Temporal variability of smoke plume height

Many studies of individual prescribed burns have found time fluctuations with smoke plumes. For example, Lavrov *et al.*

(2006) scanned a smoke plume from an experimental prescribed burn of ~1.01 ha (~2.5 acres) with a LiDAR and found double peaks in horizontal distribution of smoke particle concentrations. Simulations with a Reynolds-averaged Navier–Stokes fluid dynamical model showed fluctuations with time. The present study provides detailed features of fluctuations for multiple prescribed burns. The new finding indicates that the temporal smoke fluctuations include fast and uniform fluctuations at the time scales of minutes for almost all burns and slow and irregular fluctuations at the scales of tens of minutes to hours for some burns.

Martucci *et al.* (2010) found that the salient frequency of daytime thermal updrafts and downdrafts averaged over five cases was 2.6 mHz (equivalent to a time scale of 6.5 min). This suggests that the fluctuations of thermal processes in the PBL could be one of the causes for the fast and uniform fluctuations in the smoke plume observed in this study. The fluctuations in smoke plume height at longer scales could be related to a combination of the ignition times and methods, amount of fuel that is available (dry enough) to burn at that moment, the amount of fuel contained in the ecosystem, antecedent and current fire weather (i.e. humidity, wind, temperature) and atmospheric processes. Fire ignition is often conducted intermittently. Consequently, smoke particles can enter the atmosphere as a series of puffs or cells and buoyancy can change due to temporal changes in burn behaviour. Small-scale turbulence, variations in wind direction and speed, changes in vertical stability and changes in the internal boundary layer due to surface roughness also contribute to particulate-mass fluctuations within the smoke plume. In a PBL without strong winds, the smoke plume can be well organised and rise vertically with strong buoyancy generated from heat energy released during burning. The plume stops rising when encountering a strong inversion, reaching temperature equilibrium with the surrounding atmosphere, or entraining enough ambient air (through wind and turbulent mixing) so that it loses its initial buoyancy.

The scales of smoke plume height fluctuations show dependence on time, that is, certain scales may be remarkable only at some times of the burning period. Fuels are often heterogeneous within a burned area and the fuels to be burned can be different at various burning stages. So are the atmospheric conditions. The differences may be responsible for the time dependence of scales. This feature is useful for understanding the effects of fuel, fire behaviour and atmospheric processes on smoke dynamics. If temporal variations of fire behaviour and atmospheric conditions are known, it would be possible to understand the mechanisms for the fluctuations from the variations.

The effect of canopy is another important factor that needs to be included in smoke plume models. Vegetation can affect turbulence, buoyancy and heat transfer within smoke near the ground and therefore, dispersion and transport of smoke. This role has been examined recently in, for example, Kiefer *et al.* (2011). A canopy sub-model was developed for a regional atmospheric prediction system and used to simulate the effects of forest vegetation on the atmospheric boundary-layer dynamics and the smoke plume from a prescribed fire. The ground tower measurements indicated fast fluctuations in the meteorological fields. Given the complex mechanisms for the fluctuations within smoke plumes, smoke plume models will need to

describe multiple processes or effects of fuel, ignition, canopy, turbulence and atmospheric thermodynamics. The smoke measurements from this study could provide additional information for evaluating simulation of vegetation–atmosphere–smoke interactions. The fast and irregular fluctuations in smoke plume height affect both small-scale modelling of specific plumes and large-scale chemical transport modelling. The type of LiDAR data provided here can serve to both improve current models and to verify modelled results.

Satellite remote sensing has emerged as a useful technique to detect and monitor wildland fires and smoke. There has been limited exploration of the potential for satellite data to detect small and cool burning fires (e.g. Wang *et al.* 2007). Nonetheless, in comparison to wildfires, prescribed fires are typically smaller in terms of area burned, fireline length, and fire intensity and life time, all of which inhibit the ability of satellite instruments to detect them. Additionally, prescribed burning is often in the understorey vegetation, which further hampers detection from space. Satellite instruments are not currently able to detect smoke fluctuations or to consistently view smoke plume development and dynamics. Satellite data such as Moderate Resolution Imaging Spectroradiometer (MODIS), CALIOP, Geostationary Operational Environmental Satellites (GOES) and MISR are often able to capture smoke plumes during overhead passes within the resolution of the instruments. Smoke plume injection height can be identified with MISR (morning only overpass) and CALIOP (low temporal frequency and horizontal resolution) data. MISR and CALIOP are both global products and could provide the statistics necessary to calculate maximum, mean and minimum plume heights within large-scale ecosystems. A MISR product is available (Val Martin *et al.* 2010) and a CALIOP plume height product is under development (http://misr.jpl.nasa.gov/getData/accessData/MisrMinxPlumes/, accessed 9 September 2012). Thus, even though satellite data could provide statistics, they are not complete for detailed modelling of plume evolution and dynamics.

Vertical structure

The vertical profile of smoke plume mass is another property in addition to plume rise that is required by regional air quality models such as CMAQ. The vertical profiles measured in this study are expected to be useful for evaluating smoke dynamics modelling with smoke models such as Daysmoke. The vertical profiles averaged over the ceilometer measurement period show that approximately half of the 20 burns had more intense backscatter signals and therefore larger PM concentrations in the lower portion of the smoke plume nearer the ground than in the upper portion of the smoke plume. However, occurrences of denser smoke on the ground or in the lower portion of the smoke plume were observed by the measurement crew only for a few burns and mostly only for brief periods during the measurements. This suggests that the ceilometer might overestimate smoke density in the lower portion of smoke plumes while over-attenuating smoke signals in the upper portion. Tsai *et al.* (2009) indicated that backscatter signals from a CL31 ceilometer were more intense than those from a radar in the lower portion of a smoke plume, but were strongly attenuated above 1 km. The ceilometer backscatter signal intensity is determined by three height-dependent factors: extinction coefficient of atmospheric particles, backscatter coefficient and height normalisation (inversely proportional to the square of the height in a clear atmosphere) (Vaisala, see www.vaisala.com, accessed 26 August 2012). More calibrations of these parameters for smoke particles are needed. Note that, despite the possible over-excessive attenuation in the upper portion of a smoke plume, the ceilometer received a sufficient amount of backscatter at the top of the plume for determining height.

The enhanced optics and electronics of the CL31 ceilometer enable it to detect boundary-layer height with high resolution (Münkel *et al.* 2007). Several methods for retrieving mixing-layer height from LiDAR backscatter profiles have been presented (Menut *et al.* 1999; Steyn *et al.* 1999; Cohn and Angevine 2000; Davis *et al.* 2000), and are based on a sudden change in either backscatter or its gradient at the top of the mixing layer. Similar variations were seen in the present study at certain times during the measurement period for some burns (e.g. Fig. 4 (F3–F5), Fig. 5 (O2–O3) and Fig. 6 (E7–E8)). However, it is difficult to identify the PBL height for many other burn cases. All the burns were conducted in rural areas or near small towns where the background pollutants were much less dense than those in urban areas. In addition, most burns happened in the afternoon when the PBL during this time of year was likely to be collapsing and the background pollutants might be hard to separate from the smoke particles.

Smoke and clouds

This study recorded two cases where clouds seemed to have developed during vertical expansion and upward movement of the smoke plume. This provides new evidence for a possible role of smoke in atmospheric moist processes such as clouds and dense fog, as suggested by previous studies. Radke *et al.* (2001) proposed using clouds as part of the prescription for scheduling biomass fires because clouds and precipitation are the principal mechanisms by which the atmosphere is cleansed of particulate pollution, aerosols and smoke. The observed clouds in this study, however, appeared without producing precipitation. In this case, the smoke-generated clouds from those prescribed burns affected smoke dispersion and transport processes, but they were not developed enough to precipitate and remove smoke particles from the atmosphere. There have been numerous studies to date that suggest biomass burning can influence and potentially alter patterns of rainfall (not necessarily act as cloud concentration nuclei to stimulate rainfall). Uncertainties in the relationship between smoke, precipitation and cloud cover have also been highlighted (Andreae *et al.* 2004; Koren *et al.* 2004; Kaufman *et al.* 2005; Kaufman and Koren 2006).

Conclusions

Measurements and analyses have been taken for 20 prescribed burns in the south-eastern US using a ceilometer. The average plume height was ∼1 km. When models or measurements are not available, fire managers could use the results as an empirical guideline to estimate smoke plume height in the south-eastern US. The average height could be used as a first-order approximation for smoke plume height for prescribed burns in this region. A second-order approximation could be used by making seasonal adjustment for this region based on the increasing trend

of smoke plume heights from winter to summer. Higher-order approximations could be obtained by further making adjustments by considering hours of the day, cloud height, temperature, background wind and other fuel and fire weather variables. This approach is similar to the one used in developing the Western Regional Air Partnership (2005) plume rise scheme. Of course, actual plume height shows large variability between and within burns, even for those in the same season and ecosystem. Smoke plume models are needed to estimate more accurate plume height of a specific burn, and data from this study can be used both to verify and refine models.

Smoke particle concentrations near the burn sites are large in the PBL. The average $PM_{2.5}$ and PM_{10} concentrations within smoke plumes calculated based on the ceilometer backscatter signals are ~80 and 90 μg m^{-3}. On average the $PM_{2.5}$ and PM_{10} concentrations decrease from winter to summer. This seasonal trend may be related to the increasing trend in plume height from winter to summer. Further research is needed to understand the roles of fuel property, burn technique and atmospheric conditions.

Almost all burns show fast and uniform fluctuations at minute scales. A substantial number of burns also show slow and irregular fluctuations at scales from tens of minutes to hours, which increases the degree of difficulty in detecting prescribed-burn smoke using satellite data because the detected smoke plume height may vary considerably from one time to another. Fluctuations are influenced by complex burn and atmospheric processes. Further research is needed to understand the detailed connections.

The smoke plumes have varied vertical profiles. Large backscatter signals are found in the lower portion of smoke plumes for many burns. More inter-comparison studies with different detection techniques will help understand if this is a realistic feature of smoke plumes or is caused by under-attenuation of smoke signals at lower elevations with ceilometer detection, as found in a previous study.

The measured smoke plume height data will be used to evaluate Daysmoke. They will also be used to formulate a semi-empirical scheme to estimate smoke plume height, as was done by Harrison and Hardy (2002). The relationships between the measured smoke plume heights and fuel and atmospheric conditions (temperature, moisture, winds, etc.) will be established using statistical and similarity analysis techniques. These conditions are available to fire managers. Such schemes therefore should be practically useful for fire managers to estimate smoke plume height of prescribed burns, which will provide important information for further estimating smoke dispersion and transport to remote areas. Such schemes could also be used to assess smoke-air-quality effect simulations with regional air-quality models such as CMAQ and wildfire smoke effect models such as BlueSky.

Acknowledgement

References

Achtemeier GL (1998) Predicting dispersion and deposition of ash from burning cane. *Sugar Cane* **1**, 17–22.

Achtemeier LG (2009) On the formation and persistence of super fog in woodland smoke. *Meteorological Applications* **16**, 215–225. doi:10.1002/MET.110

Achtemeier GL, Goodrick SA, Liu YQ, Garcia-Menendez F, Hu Y, Odman MT (2011) Modeling smoke from wildland fires: plume-rise and smoke dispersion from Southern United States prescribed burns. *Atmosphere* **2**, 358–388. doi:10.3390/ATMOS2030358

Amiridis V, Giannakaki E, Balis DS, Gerasopoulos E, Pytharoulis I, Zanis P, Kazadzis S, Melas D, Zerefos C (2010) Smoke injection heights from agricultural burning in Eastern Europe as seen by CALIPSO. *Atmospheric Chemistry and Physics* **10**, 11 567–11 576. doi:10.5194/ACP-10-11567-2010

Anderson HE (1982) Aids to determining fuel models for estimating fire behavior. USDA Forest Service, Intermountain Forest and Range Experimental Station, General Technical Report INT-GTR-122. (Ogden, UT)

Andreae MO, Rosenfeld D, Artaxo P, Costa AA, Frank GP, Longo KM, Silva-Dias MAF (2004) Smoking rain clouds over the Amazon. *Science* **303**, 1337–1342. doi:10.1126/SCIENCE.1092779

Banta RM, Olivier LD, Holloway ET, Kropeli RA, Bartram BW, Cupp RE, Post MJ (1992) Smoke-column observations from two forest fires using Doppler LiDAR and Doppler radar. *Journal of Applied Meteorology* **31**, 1328–1349. doi:10.1175/1520-0450(1992)031<1328:SCOFTF>2.0.CO;2

Briggs GA (1975) Plume rise predictions. In 'Lectures on Air Pollution and Environmental Impact Analysis'. (Ed. DA Haugen) pp. 59–111. (American Meteorological Society: Boston, MA)

Byun DW, Ching J (1999) Science algorithms of the EPA Model-3 community multiscale air quality (CMAQ) modeling system. US Environmental Protection Agency, National Exposure Research Laboratory, EPA/600/R-99/030. (Research Triangle Park, NC)

Byun D, Schere KL (2006) Review of the governing equations, computational algorithms, and other components of the Models-3 Community Multiscale Air Quality (CMAQ) modeling system. *Applied Mechanics Reviews* **59**, 51–77. doi:10.1115/1.2128636

Cohn SA, Angevine WM (2000) Boundary-layer height and entrainment zone thickness measured by LiDARs and wind-profiling radars. *Journal of Applied Meteorology* **39**, 1233–1247. doi:10.1175/1520-0450(2000) 039<1233:BLHAEZ>2.0.CO;2

Colarco PR, Schoeberl MR, Doddrodge BG, Marufu LT, Torres O, Welton EJ (2004) Transport of smoke from Canadian forest fires to the surface near Washington, DC. *Journal of Geophysical Research* **109**, D06203. doi:10.1029/2003JD004248

Davis KJ, Gamage N, Hagelberg CR, Kiemle C, Lenschow DH, Sullivan PP (2000) An objective method for deriving atmospheric structure from airborne LiDAR observations. *Journal of Atmospheric and Oceanic Technology* **17**, 1455–1468. doi:10.1175/1520-0426(2000)017<1455: AOMFDA>2.0.CO;2

Diner DJ, Nelson DL, Chen Y, Kahn RA, Logan J, Leung F, Val Martin M (2008) Quantitative studies of wildfire smoke injection heights with the Terra Multi-angle Imaging Spectroradiometer. *Proceedings of SPIE* **7089**, 708908. doi:10.1117/12.795215

Freitas SR, Longo KM, Chatfield R, Latham D, Silva Dias MAF, Andreae MO, Prins E, Santos JC, Gielow R, Carvalho Jr JA (2007) Including the sub-grid scale plume rise of vegetation fires in low resolution

atmospheric transport models. *Atmospheric Chemistry and Physics* **7**, 3385–3398. doi:10.5194/ACP-7-3385-2007

Freitas SR, Longo KM, Trentmann J, Latham D (2010) Technical Note: Sensitivity of 1-D smoke plume rise models to the inclusion of environmental wind drag. *Atmospheric Chemistry and Physics* **10**, 585–594. doi:10.5194/ACP-10-585-2010

Grell G, Freitas SR, Stuefer M, Fastet J (2011) Inclusion of biomass burning in WRF-Chem: impact of wildfires on weather forecasts. *Atmospheric Chemistry and Physics* **11**, 5289–5303. doi:10.5194/ACP-11-5289-2011

Guldberg PH (1975) A comparison study of plume rise formulas applied to tall stack data. *Journal of Applied Meteorology* **14**, 1402–1405. doi:10.1175/1520-0450(1975)014<1402:ACSOPR>2.0.CO;2

Hardy C, Ferguson SA, Speers-Hayes P, Doughty CB, Teasdale DR (1993) Assessment of PUFF: a dispersion model for smoke management. USDA Forest Service, Pacific Northwest Region, Final Report. (Seattle, WA)

Harrison H, Hardy C (2002) Plume rise from gigawatt fires: observations and models. Available at http://www.atmos.washington.edu/~harrison/reports/plume3.pdf [Verified 25 August 2012]

Houyoux M, Vukovich J, Seppanen C, Brandmeyer JE (2002) SMOKE User Manual. MCNC Environmental Modeling Center. (Research Triangle Park, NC)

Jones TA, Christopher SA (2008) Variability of Georgia and Florida air quality as a function of radar derived aerosol coverage and height. In '15th Joint Conference on the Applications of Air Pollution Meteorology', 20–24 January 2008, New Orleans, LA. Paper J1.3. (American Meteorological Society: Boston, MA)

Kahn RA, Li WH, Moroney C, Diner DJ, Martonchik JV, Fishbein E (2007) Aerosol source plume physical characteristics from space-based multiangle imaging. *Journal of Geophysical Research* **112**, D11205. doi:10.1029/2006JD007647

Kahn RA, Chen Y, Nelson DL, Leung FY, Li Q, Diner DJ, Logan JA (2008) Wildfire smoke injection heights–two perspectives from space. *Geophysical Research Letters* **35**, L04809. doi:10.1029/2007GL032165

Kaufman YJ, Koren I (2006) Smoke and pollution aerosol effect on cloud cover. *Science* **313**, 655–658. doi:10.1126/SCIENCE.1126232

Kaufman YJ, Koren I, Remer LA, Rosenfeld D, Rudich Y (2005) The effect of smoke, dust, and pollution aerosol on shallow cloud development over the Atlantic Ocean. *Proceedings of the National Academy of Sciences of the United States of America* **102**, 11 207–11 212. doi:10.1073/PNAS.0505191102

Kiefer MT, Heilman WE, Zhong S, Charney JJ, Bian X, Shadbolt RP, Hom JL, Clark KL, Skowronski N, Gallagher M, Patterson M (2011) Development of a fine scale smoke dispersion modeling system: part II – case study of a prescribed burn in the New Jersey Pine Barrens. In 'Ninth Symposium on Fire and Forest Meteorology', 18–21 October 2011, Palm Springs, CA. (Eds BE Potter, TJ Brown) (American Meteorological Society) Available at http://ams.confex.com/ams/9FIRE/webprogram/9FIRE.html [Verified 25 August 2012]

Koren I, Kaufman YJ, Remer LA, Martins JV (2004) Measurement of the effect of Amazon smoke on inhibition of cloud formation. *Science* **303**, 1342–1345. doi:10.1126/SCIENCE.1089424

Kovalev VA, Petkov A, Cyle W, Urbanski S, Hao WM (2009) Determination of smoke plume and layer heights using scanning LiDAR data. *Applied Optics* **48**(28), 5287–5294. doi:10.1364/AO.48.005287

Labonne M, Breon FM, Chevallier F (2007) Injection height of biomass burning aerosols as seen from a spaceborne LiDAR. *Geophysical Research Letters* **34**, L11806. doi:10.1029/2007GL029311

Larkin NK, O'Neill S, Solomon R, Raffuse S, Strand T, Sullivan DC, Krull C, Rorig M, Peterson J, Ferguson S (2009) The BlueSky smoke modeling framework. *International Journal of Wildland Fire* **18**, 906–920. doi:10.1071/WF07086

Latham D (1994) PLUMP: a one-dimensional plume predictor and cloud model for fire and smoke managers. USDA Forest Service, Intermountain Research Station, General Technical Report INT-GTR-314. (Missoula, MT)

Lavrov A, Utkin A, Vilar R, Fernandes A (2003) Application of LiDAR in ultraviolet, visible and infrared ranges for early forest fire detection. *Applied Physics B, Lasers and Optics* **76**, 87–95. doi:10.1007/S00340-002-1053-Y

Lavrov A, Utkin AB, Vilar R, Fernandes A (2006) Evaluation of smoke dispersion from forest fire plumes using LiDAR experiments and modelling. *International Journal of Thermal Sciences* **45**, 848–859. doi:10.1016/J.IJTHERMALSCI.2006.01.003

Liu YQ (2005) Land breeze and thermals: a scale threshold to distinguish their effects. *Advances in Atmospheric. Science* **22**(6), 889–902. doi:10.1007/BF02918688

Liu YQ, Goodrick SL, Achtemeier GL, Jackson WA, Qu J, Wang W (2009) Smoke incursions into urban areas: simulation of a Georgia prescribed burn. *International Journal of Wildland Fire* **18**, 336–348. doi:10.1071/WF08082

Liu YQ, Achtemeier GL, Goodrick GL, Jackson WA (2010) Important parameters for smoke plume rise simulation with Daysmoke. *Atmospheric Pollution Research* **1**, 250–259. doi:10.5094/APR.2010.032

Mandel J, Beezley JD, Kochanski AK (2011) Coupled atmosphere-wildland fire modeling with WRF 3.3 and SFIRE 2011. *Geoscientific Model Development* **4**(3), 591–610. doi:10.5194/GMD-4-591-2011

Martucci G, Matthey R, Mitev V, Richner H (2010) Frequency of boundary-layer top fluctuations in convective and stable conditions using laser remote sensing. *Boundary-Layer Meteorology* **135**, 313–331. doi:10.1007/S10546-010-9474-3

McKendry IG, Gallagher J, Campuzano P, Bertram A, Strawbridge K, Leaitch R, Macdonald AM (2010) Ground-based remote sensing of an elevated forest fire aerosol layer. *Atmospheric Chemistry and Physics* **10**, 11 921–11 930. doi:10.5194/ACP-10-11921-2010

Melnikov VM, Zrnic DS, Rabin RM, Zhang P (2008) Radar polarimetric signatures of fire plumes in oklahoma. *Geophysical Research Letters* **35**, L14815. doi:10.1029/2008GL034311

Menut L, Flamant C, Pelon J, Flamant PH (1999) Urban boundary-layer height determination from LiDAR measurements over the Paris area. *Applied Optics* **38**, 945–954. doi:10.1364/AO.38.000945

Meyer Y (1993) 'Wavelets: Algorithms and Applications.' (SIAM: Philadelphia, PA)

Markowicz KM, Flatau PJ, Kardas AE, Remiszewskaj J, Stelmaszcyk K, Wöste L (2008) Ceilometer retrieval of the boundary layer vertical aerosol extinction structure. *Journal of Atmospheric and Oceanic Technology* **25**, 928–944. doi:10.1175/2007JTECHA1016.1

Mikkelsen T, Jorgensen HE, Nielsen M, Ott S (2002) Similarity scaling of surface-released smoke plumes *Boundary-Layer Meteorology* **105**, 483–505. doi:10.1023/A:1020380820526

Morlet J, Arens G, Fourgeau E, Griad D (1982*a*) Wave propagation and sampling theory – part 1: complex signal and scattering in multilayered media. *Geophysics* **47**, 203–221. doi:10.1190/1.1441328

Morlet J, Arens G, Fourgeau E, Griad D (1982*b*) Wave propagation and sampling theory – part 2: sampling theory and complex waves. *Geophysics* **47**, 222–236. doi:10.1190/1.1441329

Müller D, Mattis I, Wandinger V, Ansmann A, Althausen D, Stohl A (2005) Raman LiDAR observations of aged Siberian and Canadian forest fire smoke in the free troposphere over Germany in 2003: microphysical particle characterization. *Journal of Geophysical Research* **110**, D17201. doi:10.1029/2004JD005756

Münkel C, Emeis S, Müller WJ, Schäfer K (2004) Aerosol concentration measurements with a LiDAR ceilometer: results of a one year measuring campaign. *Proceedings of SPIE* **5235**, 486–496. doi:10.1117/12.511104

Münkel C, Eresmaa N, Räsänen A, Karppinen A (2007) Retrieval of mixing height and dust concentration with LiDAR ceilometer. *Boundary-Layer Meteorology* **124**, 117–128. doi:10.1007/S10546-006-9103-3

Pershin S, Hao WM, Susott RA, Babbitt RE, Riebau A (1999) Estimation of emission from Idaho biomass fires using compact eye-safe diode LiDAR. *Proceedings of SPIE* **3757**, 60–66. doi:10.1117/12.366438

Potter BE (2005) The role of released moisture in the atmospheric dynamics associated with wildland fires. *International Journal of Wildland Fire* **14**, 77–84. doi:10.1071/WF04045

Pouliot G, Pierce T, Benjey W, O'Neill SM, Ferguson SA (2005) Wildfire emission modeling: integrating BlueSky and SMOKE. In '14th Annual International Emission Inventory Conference', 11–14 April 2005, Las Vegas, NV. (US Environmental Protection Agency: Research Triangle Park, NC) Available at http://www.epa.gov/ttn/chief/conference/ei14/session12/pouliot.pdf [Verified 25 August 2012]

Radke LF, Ward DE, Philip J, Riggan PJ (2001) A prescription for controlling the air pollution resulting from the use of prescribed biomass fire: clouds. *International Journal of Wildland Fire* **10**, 103–111. doi:10.1071/WF01020

Raffuse S, Wade K, Stone J, Sullivan D, Larkin N, Tara S, Solomon R (2009) Validation of modeled smoke plume injection heights using satellite data. In 'Eighth Symposium on Fire and Forest Meteorology', 12–15 October 2009, Kalispell, MT. (Eds BE Potter, TJ Brown) Paper 5A.3. (American Meteorological Society) Available at https://ams.confex.com/ams/8Fire/techprogram/paper_156192.htm [Verified 26 August 2012]

Riebau AR, Fox D (2010) The Joint Fire Science Program Smoke Science Plan. JFSP project 1–C-01–01 Available at http://www.firescience.gov/documents/smoke/2010_JFSP_Smoke_Science_Plan_Final_Version_without_Appendix_B_1.0.pdf [Verified 26 August 2012]

Rogers RR, Brown WOJ (1997) Radar observation of a major industrial fire. *Bulletin of the American Meteorological Society* **78**, 803–814. doi:10.1175/1520-0477(1997)078<0803:ROOAMI>2.0.CO;2

Skamarock WC, Klemp JB, Dudhia J, Gill DO, Barker DM, Duda MG, Huang X-Y, Wang W, Powers JG (2008) A description of the advanced research WRF Version 3, NCAR Technical Note 475, available at: http://www.mmm.ucar.edu/wrf/users/docs/arwv3.pdf [Verified 26 August 2012]

Stein AF, Rolph GD, Draxler RR, Stunder B, Ruminski M (2009) Verification of the NOAA smoke forecasting system: model sensitivity to the injection height. *Weather and Forecasting* **24**, 379–394. doi:10.1175/2008WAF2222166.1

Steyn DG, Baldi M, Hoff RM (1999) The detection of mixed layer depth and entrainment zone thickness from LiDAR backscatter profiles.

Journal of Atmospheric and Oceanic Technology **16**, 953–959. doi:10.1175/1520-0426(1999)016<0953:TDOMLD>2.0.CO;2

Torrence C, Compo GP (1998) A practical guide to wavelet analysis. *Bulletin of the American Meteorological Society* **79**, 61–78. doi:10.1175/1520-0477(1998)079<0061:APGTWA>2.0.CO;2

Trentmann J, Andreae MO, Graf H-F, Hobbs PV, Ottmar RD, Trautmann T (2002) Simulation of a biomass-burning plume: Comparison of model results with observations. *Journal of Geophysical Research* **107**, 4013. doi:10.1029/2001JD000410

Tsai PS, Frasier SJ, Goodrick S, Achtemeier G, Odman MT (2009) Combined LiDAR and radar observations of smoke plumes from prescribed burns. In 'Fourth Symposium on LiDAR Atmospheric Applications', 10–16 January 2009, Phoenix, AZ. (Eds BB Demoz, J Comstock, A Behrendt) Paper 2.1. (American Meteorological Society) Available at https://ams.confex.com/ams/89annual/techprogram/paper_147257.htm [Verified 26 August 2012]

Tsaknakis G, Papayannis A, Kokkalis P, Amiridis V, Kambezidis HD, Mamouri RE, Georgoussis G, Avdikos G (2011) Inter-comparison of LiDAR and ceilometer retrievals for aerosol and Planetary Boundary Layer profiling over Athens, Greece. *Atmospheric Measurement Techniques* **4**, 1261–1273. doi:10.5194/AMT-4-1261-2011

Val Martin M, Logan JA, Kahn RA, Leung FY, Nelson DL, Diner DJ (2010) Smoke injection heights from fires in North America: analysis of 5 years of satellite observations. *Atmospheric Chemistry and Physics* **10**, 1491–1510. doi:10.5194/ACP-10-1491-2010

Wade DD, Brock BL, Brose PH, Grace JB, Hoch GA, Patterson WA III (2000) Fire in eastern ecosystems. In 'Wildland Fire in Ecosystems: Effects of Fire on Flora'. (Eds JK Brown, JK Smith) USDA Forest Service, Rocky Mountain Research Station, General Technical Report RMRS-42, Ch. 4, vol. 2, pp. 53–96. (Ogden, UT)

Wang WT, Qu J, Hao XJ, Liu YQ, Sommers WT (2007) An improved algorithm for small and cool fire detection using MODIS data: a preliminary study in the southeastern United States. *Remote Sensing of Environment* **108**(2), 163–170. doi:10.1016/J.RSE.2006.11.009

Weil JC (1988) Plume rise. In 'Lectures on Air Pollution Modeling'. (Eds A Venkatram, JC Wyngaard). pp. 119–166. (American Meteorological Society: Boston, MA)

Winker D, Vaughan M, Hunt W (2006) The CALIPSO mission and initial results from CALIOP. *Proceedings of the Society for Photo-Instrumentation Engineers* **6409**, 640902. doi:10.1117/12.698003

Western Regional Air Partnership (2005) 2002 Fire emission inventory for the WRAP Region Phase II. Essential Documentation. (Air Sciences, Inc.) Available at http://www.wrapair.org/forums/fejf/documents/wrap_2002_phii_ei_report_20050722.pdf [Verified 26 August, 2012]